Composites: Part A 140 (2021) 106181

Contents lists available at ScienceDirect

Composites Part A

journal homepage: www.elsevier.com/locate/compositesa

Load-dependent path planning method for 3D printing of continuous fiber reinforced plastics

Ting Wang [a], Nanya Li [a,*], Guido Link [a], John Jelonnek [a], Jürgen Fleischer [b], Jörg Dittus [b], Daniel Kupzik [b]

[a] Institute for Pulsed Power and Microwave Technology, Karlsruhe Institute of Technology, Eggenstein-Leopoldshafen 76344, Germany
[b] wbk Institute of Production Science, Karlsruhe Institute of Technology, Karlsruhe 76131, Germany

ARTICLE INFO

Keywords:
Load-dependent path planning
Continuous fiber reinforcement
Stress vector tracing
3D printing

ABSTRACT

3D printing, to print continuous fiber reinforced plastics (CFRPs) has advantages of manufacturing complex shape and short production cycle. Due to anisotropic mechanical properties of continuous fibers, the paving direction of the fibers determines the mechanical strengths of the printed CFRPs. In this paper, a novel load-dependent path planning (LPP) method has been proposed to generate printing path for CFRPs, which exactly follows the load transmission path of the parts and could provide higher mechanical properties. A topology optimization method is applied to simplify the original disordered load distribution. In the developed Stress Vector Tracing (SVT) algorithm, the printing paths are generated along the load transmission path with the variable spacing of adjacent paths. The LPP method has been compared with the state-of-the-art printing path planning method for continuous fibers and shown better load-bearing and printability.

1. Introduction

Fused filament fabrication (FFF) of thermoplastic materials has advantages of low costs and short production cycle [1]. Generally, filaments are extruded through a hot-end of a nozzle and deposited on a printing platform to build a geometry layer-by-layer [2]. Due to higher strength and lightweight features, the continuous fiber exhibits enormous potential to enhance the plastic parts [3,4]. Three kinds of 3D printing technologies are commonly used in the manufacturing of continuous fiber reinforced polymer composites, as shown in Fig. 1. For the methods exhibited in Fig. 1(a) and (b), the composite filaments are impregnated while the printing process. The out-of-nozzle impregnation uses two feeders to simultaneously print the thermoplastic filament and continuous fiber on the printing bed [5]. The fusion of the continuous fiber and plastic are accomplished outside the nozzle. In the process of in-nozzle impregnation, the continuous fiber and thermoplastic filament are feed into a hot-end and mixed together inside [6]. In Fig. 1(c), a semi-finished CFRP filament has been fabricated as prepreg material and the heating cavity could be a conventional hot-end or a microwave resonant cavity [7]. The experimental results indicate that higher compressive properties can be obtained by using prepreg filament than other methods [8].

Recently, the continuous fiber reinforced composites manufactured by FFF can only have fibers in simple geometry and limited areas, because of lacking effective path planning method [9]. As one of the key parameters, printing path has not only the influence on the geometry but also determines the mechanical properties of the printed part with different fiber orientations [10,11]. At present, the most commonly used printing patterns of CFRPs filaments FFF are raster path [12], zigzag path [13], Hilbert-curves path, spiral-curves path [14], contour-parallel path [15] and hybrid path [16], due to their simplicity and high adaptability. However, manufacturing complex components with CFPRs requires an uninterrupted and smooth printing path to avoid breakage of fibers and improve printing quality.

The different 3D printing methods of CFRPs are compared and reviewed in Table 1. For example, Li et al. [6] researched the mechanical strength of the 3D printed CFRPs and used the zigzag-contour hybrid path to print the samples. Baumann et al. [5] compared the tensile properties of three different methods of producing fiber reinforced composites and used one-directional filling pattern to manufacture the testing samples. The contour-parallel printing pattern is also used in the manufacturing of the CFRPs testing samples [19]. Eiger software of Markforged uses zigzag-contour hybrid and concentric filling pattern for the printing process. Because the fiber reinforced filament provides

* Corresponding author.
E-mail address: nanya.li@kit.edu (N. Li).

https://doi.org/10.1016/j.compositesa.2020.106181
Received 15 August 2020; Received in revised form 7 October 2020; Accepted 24 October 2020
Available online 28 October 2020
1359-835X/

excellent self-supporting property, the three-dimensional CFRPs can be printed [28]. The printing paths optimized by stress distribution have been researched by Sugiyama et al. [30] and Li et al. [31], the preliminary research works show promising advantages to print the continuous carbon fibers along the load transmission path.

The above mentioned research achievements prove the considerable efforts in the ongoing development of 3D printing CFRPs. However, the path planning methods need further development to: 1) have an algorithm to match the printing path with load transmission; 2) generate continuous printing path to avoid damaging the continuity of stresses; 3) prevent small radius (high curvature) corner and sharp angle of the printing path which may break the continuous fiber. In this paper, a load-dependent path planning (LPP) method is developed under the consideration of principal stress distribution, fiber limitation and variable printing speed demands. Based on the topology optimization and developed Stress Vector Tracing (SVT) algorithm, the geometry is fully printed with a continuously connected fiber path. Comparisons have been done between the LPP, commercial path planning software (Slic3r) and the state-of-art path planning method of CFRPs.

2. Load-dependent path planning (LPP) method

2.1. Simplifying load distribution by topological optimization

The ply direction of continuous fibers has a significant influence on the mechanical properties of manufactured CFRPs. Apparently, the printing path of continuous fiber reinforced thermoplastic filaments plays an important role in controlling the mechanical properties of printed composites [32,33]. However, the 3D printing path planning of continuous fiber reinforced plastics has encountered bottleneck of parts with complex geometries, because of the disordered stress distribution under different load conditions. The disorganized and interrupted tensile and compressive stresses cannot be followed with a continuous path. Here, we involve a topological optimization method named Solid Orthotropic Material with Penalization (SOMP) [34] to re-arrange the original stress vectors in order. The SOMP topology optimization approach is based on the Solid Isotropic Material with Penalization (SIMP) approach, which is extended to the orthotropic material. The mechanical properties of a composite laminate [35] has been used during the topological optimization (Young's modulus: $E_1 = 18.3$ GPa; $E_2 = 19.8$ GPa, Poisson's ratio: $\nu_{12} = \nu_{21} = 0.17$, Shear modulus: $G_{12} = 5.15$ GPa). The topology optimization method with design goal of minimum compliance can be written as [36]:

Table 1
Comparison of different printing path planning methods of CFRPs.

Printing path	Material	Author
Straight line	CF-PLA	Heidari-Rarani, et al. 2019 [12]
	CF-ABS	Baumann, et al. 2017 [5]
Zigzag	CF-Nylon	Dutra, et al. 2019 [13]
	CF-Nylon	Kousiatza, et al. 2019 [17]
	CF-TPI	Ye, et al. 2019 [18]
Contour	CF-Nylon	Todoroki, et al. 2020 [19]
	CF-Nylon	Mohammadizadeh, et al. 2019 [15]
	CF-Nylon	Li, et al. 2016 [6]
Zigzag-contour hybrid	CF-Nylon	Naranjo-Lozada et al. 2019 [16]
	CF-Nylon	Ivey, et al. 2017 [20]
Honeycomb	CF-ABS	Ming, et al. 2019 [21]
	CF-Nylon	Liu, et al. 2020 [22]
	CF-PLA	Quan, et al. 2020 [23]
Spiral	CF -PLA	Akhoundi, et al. 2020 [14]
	CF-Nylon	Dickson, et al. 2017 [24]
Wavy	CF-Nylon	Adumitroaie, et al. 2019 [25]
Grid	CF-Nylon	De Backer, et al. 2020 [26]
3D lattice	CF-Nylon	Eichenhofer, et al. 2017 [27]
3D lattice	CF-PLA	Liu, et al. 2018 [28]
Curved path	CFRPs	Shembekar, et al. 2019 [29]
Optimized based on stress	CF-Nylon	Sugiyama, et al. 2020 [30]
	CF-Nylon	Li, et al. 2020 [31]

CF: continuous fiber; ABS: acrylonitrile–butadienestyrene; PLA: Polylactic acid; TPI: Thermoplastic-Polyimide.

$$min: c(\rho,\theta) = U^T K U = \sum_{e=1}^{N} [T_{min} + (\rho_e)^P (T_0 - T_{min})] u_e^T k_\theta^e u_e$$

$$subjected\ to: \begin{cases} KU = F \\ \dfrac{V(\rho)}{V^*} \leqslant f \\ \rho \in [0,1] \end{cases} \tag{1}$$

where ρ is the density, ρ_e is the density of elements, P is the penalty, θ is the fiber orientation, N is the number of design elements. U, K and F denote the global displacement, global stiffness matrix and force vector respectively. T_0 matrix consists of the properties of the orthotropic material. T_{min} is set to 10^{-3} in order to prevent any possible singularity of the equilibrium problem. u_e and k_θ^e represents the element displacement vector and the element stiffness matrix. $V(\rho)$, V^* and f are the material volume, design material volume and defined volume fraction respectively.

As shown in Fig. 2, the original design contains several data sets and boundary, including the material set ($\Omega_{material}$), load set (Ω_{load}) and

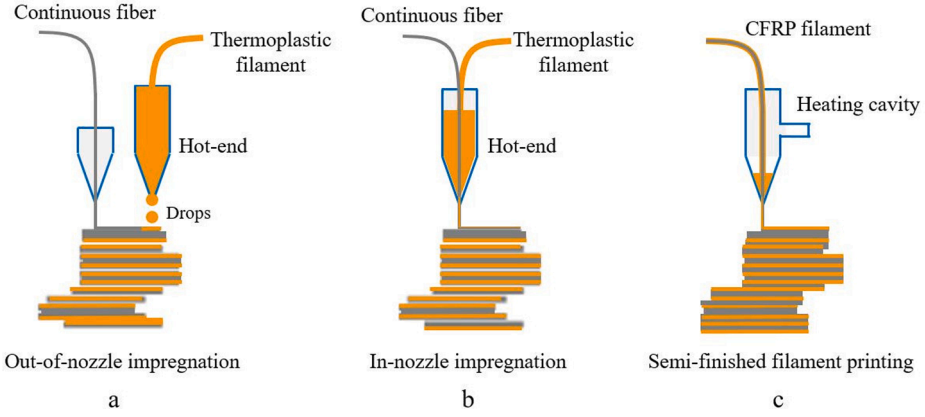

Fig. 1. Different 3D printing methods of continuous fiber reinforced plastics: (a) out-of-nozzle impregnation; (b) in-nozzle impregnation and (c) semi-finished CFRP filament printing.

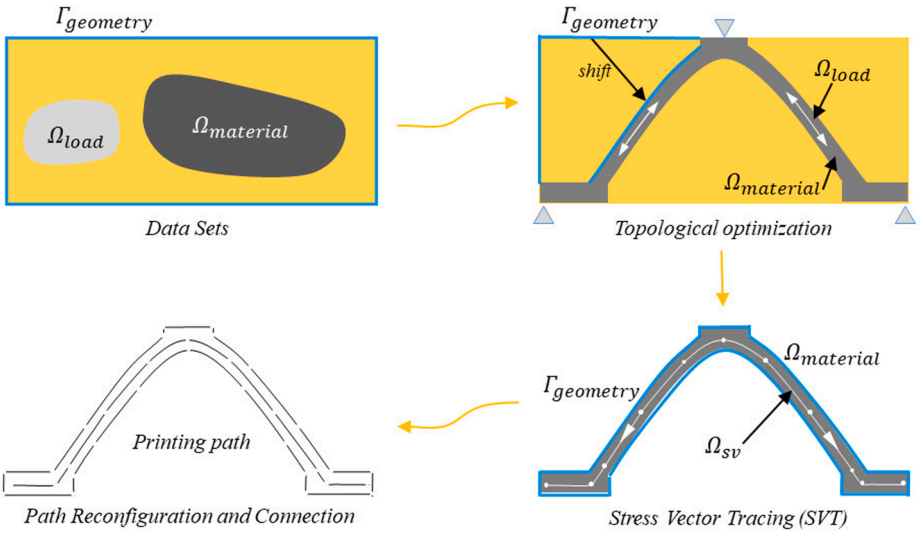

Fig. 2. Schematic of the load-dependent path planning method.

geometry boundary ($\Gamma_{geometry}$). After the topological optimization process, the geometry boundary will shift to the new areas, which have higher stress density. The material set will reshape to a structure that only has beams and scaffolds under certain external loads. Meanwhile, the tensile and compressive stress vectors can be obtained. Then, a developed stress vector tracing algorithm (detailed information is described in Section 2.2) has been used to define new geometry boundaries and coordinate the stress vector set (Ω_{sv}). A load-dependent printing path of continuous fiber reinforced plastics can be generated to have the fiber orientation follow the distribution of principal stresses.

2.2. Developing stress vector tracing (SVT) algorithm

The SVT algorithm contains medial axis extraction using Voronoi diagram [37] and vector-trace algorithm to obtain the printing paths that follow the load transmission. The medial axis extraction is to acquire geometrical features of the structure, as shown in Fig. 3. The boundary points of the structure are used as the seeds of Voronoi diagram so that the adjacent edges of sub-regions can be extracted as medial axis, and then a relationship between the medial axis points and geometrical boundary points is built. The yellow points are the geometrical boundary points, and for each two neighbor boundary points, an equidistant line called Voronoi edge is generated to divide the area between them, as shown in Fig. 3(a). With the segmentation of the Voronoi edges, the medial axis is generated and represented by the black curve located between the geometrical boundary curves, as shown in Fig. 3(b).

There are three geometrical parameters that are used in the vector-trace algorithm, as shown in Fig. 4. The angle β between path segment and nearby stress vector. The α is the angle between two adjacent path segments, and d is the distance between two nearby points. The physical meanings of these parameters represent the orientation difference between the generated path and the stress vectors, the smoothness of the path and the resolution of the generated path based on the points of medial axis. Obviously, more points of the medial axis are used, the higher resolution of the generated path is.

Ideally, the three geometrical parameters should as small as possible. Thus, an evaluation criterion has been applied to optimize these parameters. Assuming that the green path vector in Fig. 4 is v_{pl}, and the angleαbetween the v_{pn} (the next yellow vector) and v_{pl} is calculated in Eq. (2). The angle β between stress vector (v_{stress}) and v_{pn} is calculated by Eq. (3). And the distance d between two nearby points on the path is also calculated.

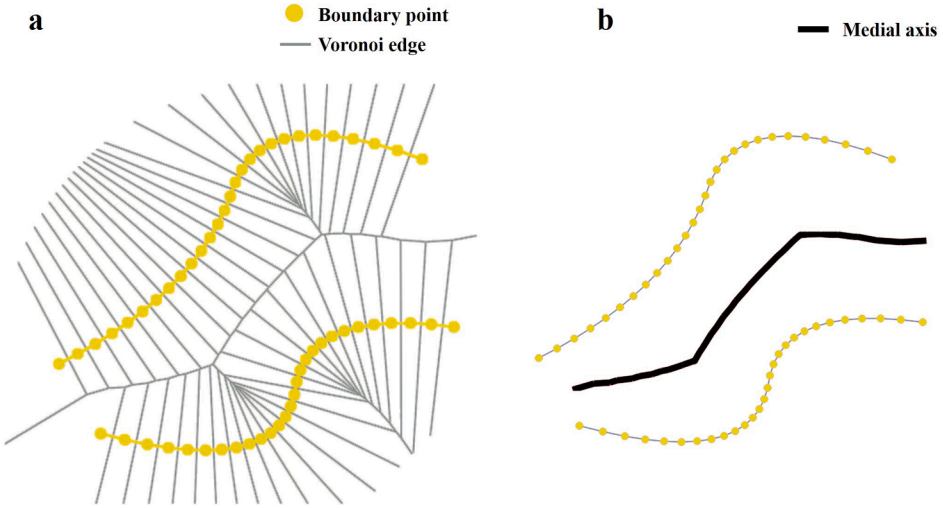

Fig. 3. Schematic of using Voronoi diagram to generate medial axis: (a) Voronoi diagram; (b) generated medial axis.

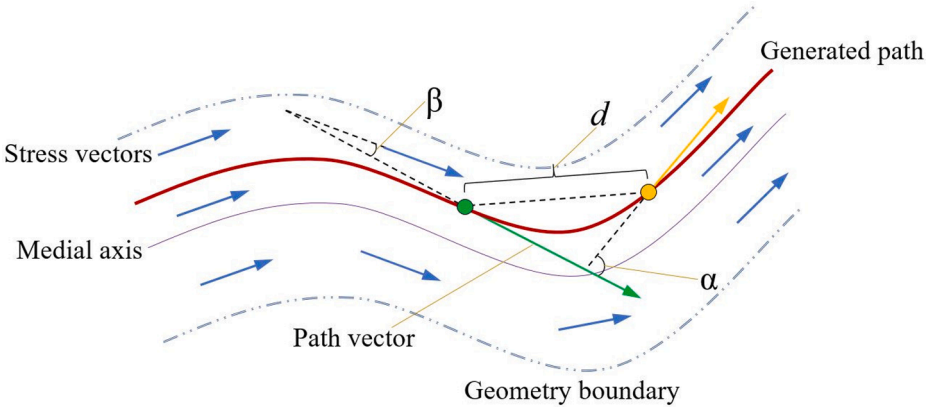

Fig. 4. Geometrical parameters that are used in vector-trace algorithm.

$$\alpha = cos^{-1}\left(\frac{v_{pl}\cdot v_{pn}}{|v_{pl}||v_{pn}|}\right) \tag{2}$$

$$\beta = cos^{-1}\left(\frac{v_{pn}\cdot v_{stress}}{|v_{pn}||v_{stress}|}\right) \tag{3}$$

There are several factors in the evaluation criterion that should be applied, including distance coefficient$\gamma(d)$, stress coefficient$\gamma(\beta)$and path coefficient$\gamma(\alpha)$. They are uniformly expressed by $\gamma(z)_{z=\alpha,\beta,z}$ in the Eq. (4), where the k_z is the amplification factor (weight factor) according to different coefficient, the η and ε are arbitrary constants that are used to change each coefficient. By multiplying the three coefficients, the coefficient of smooth δ of each point can be obtained, as shown in Eq. (5).

The coefficient of smooth of generated path has been evaluated by considering turning angle, the difference between the path and stresses, and distance between two path points. Then the point with the smallest coefficient of smooth is chosen to be the next point of the path. The algorithm is executed until there are no more medial axis points left or the search area is empty.

$$\gamma(z)_{z=\alpha,\beta,d} = \left(\frac{z}{z_{limit}}\right)\cdot\frac{(k_z\cdot\eta-\varepsilon)}{k_z}+\varepsilon \tag{4}$$

$$\delta = \prod_{z\,=\,\alpha,\beta,d}\gamma(z) \tag{5}$$

By using the SVT algorithm, the LPP with variable spacing are generated along the load transmission path. Based on the geometrical

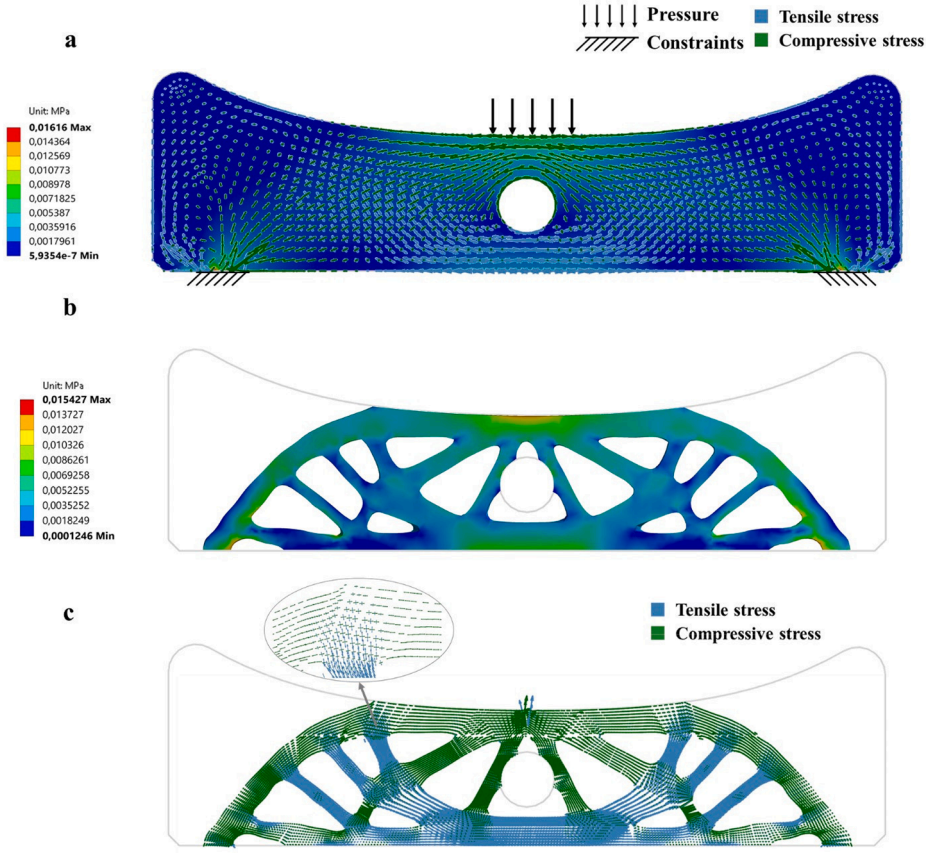

Fig. 5. Stresses analyzing of the bridge part: (a) mechanical analysis model; (b) stresses distribution after analyzing; (c) re-ordered stresses distribution inside the part.

characteristics of the printing path, different printing speeds are applied. For example, the straight lines have the highest printing speed, the curved turns should be printed with low speed, to make sure the filament can continuously adhere to the printing bed.

3. Result and discussions

3.1. LPP of CF reinforced bridge and suspension parts

In this section, a continuous fiber reinforced three-points-bending bridge and a suspension part are calculated to verify the developed path planning method. For the bridge part (width: 185 mm and height: 50 mm), an external force and two support conditions are applied as shown in Fig. 5(a). After the mechanical analyzing, the stresses distribution is reorganized (Fig. 5(b)) and the tensile and compressive stresses can be separated into different areas and always along the medial axis direction of these beams, as illustrated in Fig. 5(c).

With the help of the developed vector-trace algorithm, the tensile and compressive stresses are calculated as load paths based on the medial axis. The printing paths with variable spacing are generated inside the geometrical boundaries and connected. The geometrical adaptive printing speeds according to the curvature, angle and length of straight lines (or curves) of the printing path are shown in Fig. 6. The parameters that are used to determine the printing speed of the printing path segments are shown in Table 2.

With regarding to the curvatures of the printing path, the curvature of each point on the path has been calculated based on the angle and distance between two adjacent directional vectors. The length of the curves is also an influencing factor, because some of the curves are not long enough to accomplish the acceleration and deceleration process. Thus, a high printing speed can only be arranged to a long distance and low curvature curve without sharp turn.

In addition, it can be seen in the Fig. 6 that the load-dependent path has less curves with high curvature and they are generally located outside of the geometry boundary, which have no effect to the printed part. The curves inside the boundary have lower curvature because of the continuity of load-transmission path. That indicates the load-dependent printing path is smoother than other commercial printing paths. As shown in Fig. 7, a suspension part is studied to generate the load-dependent printing path and will be compared with the commercial path planning method. The suspension part has a 175 mm width, 126 mm height, and both of the paths of the bridge and suspension part can be shrunk or magnified. A compressive load is applied on the top of cantilever and bottom areas are fixed with supports. The stress analysis before and after the topology optimization are shown in Fig. 7(a) and (b). The main paths along the stresses transfer are generated by using the vector-trace algorithm and some segments of path are separated into different branches due to the different load-transmission directions, the result is shown in Fig. 7(c). Thus, the non-isometric printing paths in terms of the extracted load-dependent paths are generated and connected together, as shown in Fig. 7(d).

Table 2
Printing speeds according to the curvature, length of the curves and angle.

Printing speed	7 mm/s	15 mm/s	35 mm/s
Curvature κ (mm^{-1})	κ > 0.2	0.05<= κ <=0.2	κ < 0.05
Length L (mm)	L < 15	15≤ *L* ≤25	L > 25
Angle A (°)	A < 90	90<= A <=135	A >=135

3.2. Comparison of load-dependent printing path with Slic3r

The curvature of the printing path is a significant parameter for the 3D printing of CFRPs which affects directly the processing feasibility and quality of the printed part. The curvature of different printing paths of bridge part and suspension part are estimated and compared, as shown in Figs. 8 and 9 respectively. Fig. 8(a) shows the curvature distribution of the LPP printing path, and Fig. 8(b) to (d) exhibit the curvature distributions of the concentric, 45° zigzag and 90° zigzag printing paths generated by Slic3r. All of the printing paths have the similar highest value of the curvature and is about 4 mm^{-1}. The concentric printing path shown in Fig. 8(b) has many sharp curves at turning points and the curvature distribution of the 45° zigzag printing path and 90° zigzag printing path own the same tendency (shown in Fig. 8(c) and Fig. 8(d)), due to the huge amount of turns with high curvature and abrupt printing direction variation. The LPP printing path is generated by following the principal stress transfers, which is smooth due to the integrity of the force transmission path so that it has a few high curvature curves. About 80% of the curves of the LPP printing path have curvature less than 0.26 mm^{-1} (3.8 mm radius of curvature).

Furthermore, the curvature distributions of different printing paths of the suspension part are shown in Fig. 9(a) to (d), a similar result as that of the bridge part can be obtained. Significantly, the LPP printing path has only a few of high curvature curves that reach the highest value, in which about 72% of the curves have curvature less than 0.26 mm^{-1}. Meanwhile, many curves of the printing paths generated by Slic3r have reached the highest value 4 mm^{-1}. The high curvature curves of the concentric printing path are mostly located on the areas around the two holes. Moreover, the fluctuation of the curvature change of the LPP printing path has lower value and frequency than the other printing paths.

Another vital parameter of the generated printing path of CFRPs is the fiber orientation. The orientation difference between the principal

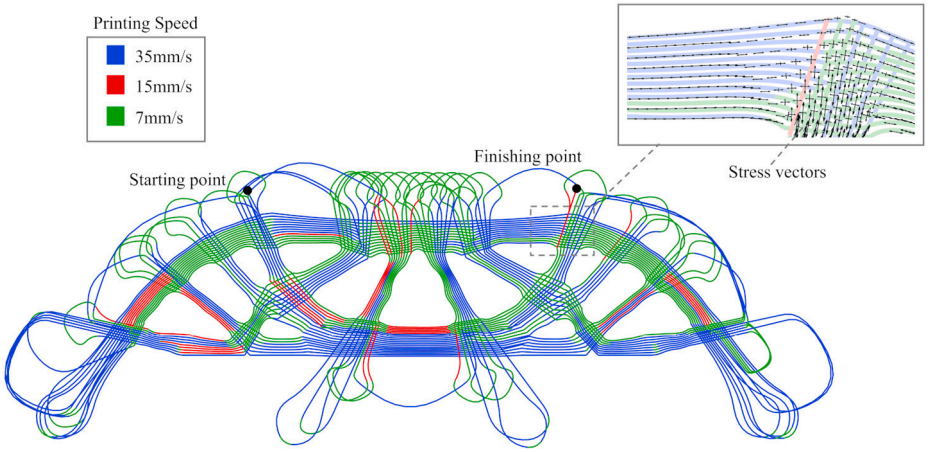

Fig. 6. Continuously connected printing path of the bridge part with variable printing speeds.

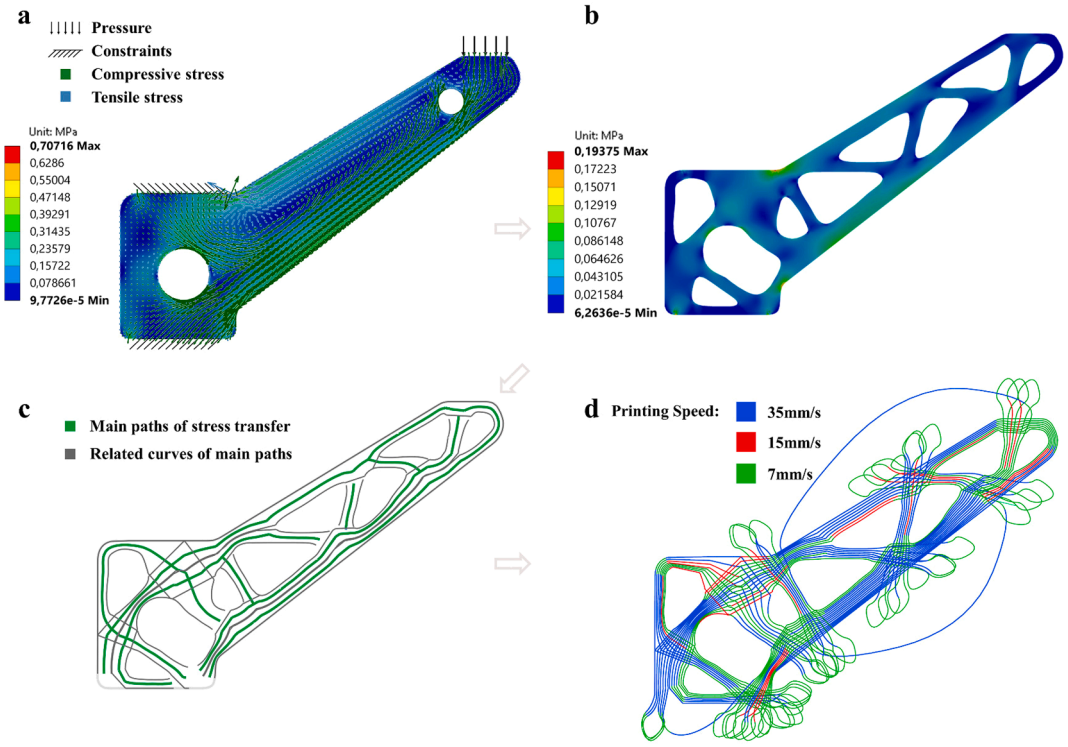

Fig. 7. Processes of generating the continuous printing path of the suspension part: (a) load and stresses distribution; (b) optimized stresses distribution and area; (c) main printing paths generated by the developed vector-trace algorithm; (d) generated continuous printing paths.

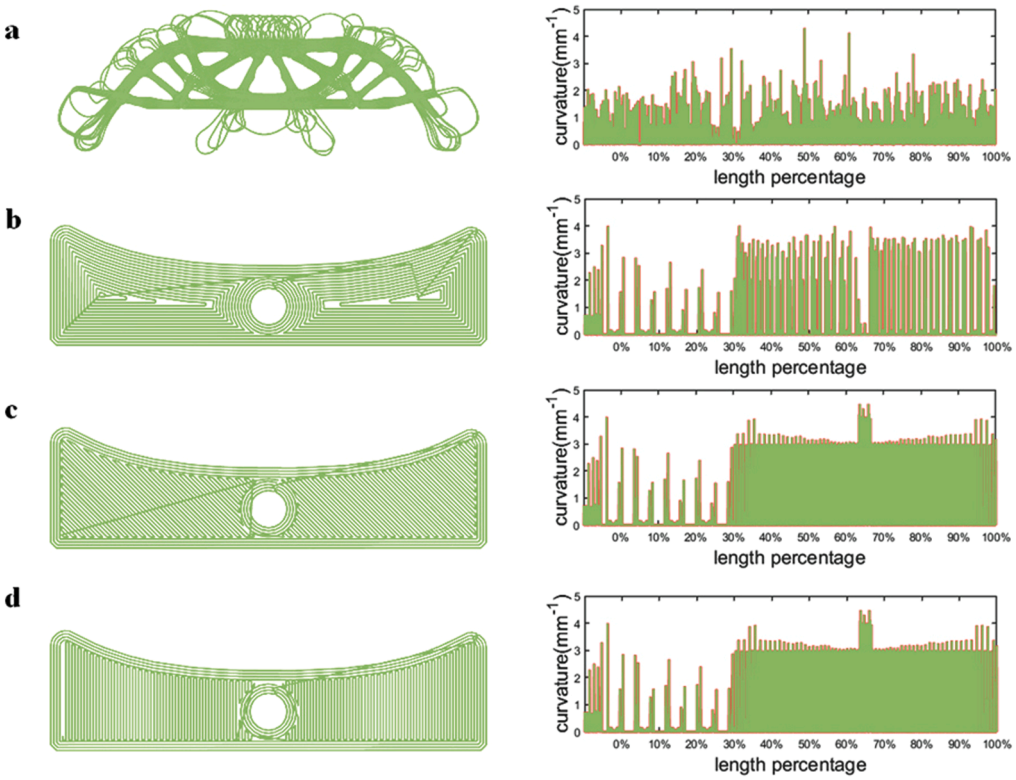

Fig. 8. Curvature distribution of different printing paths of the bridge part: (a) to (d) curvature distribution of LPP, concentric, 45° zigzag and 90° zigzag printing paths.

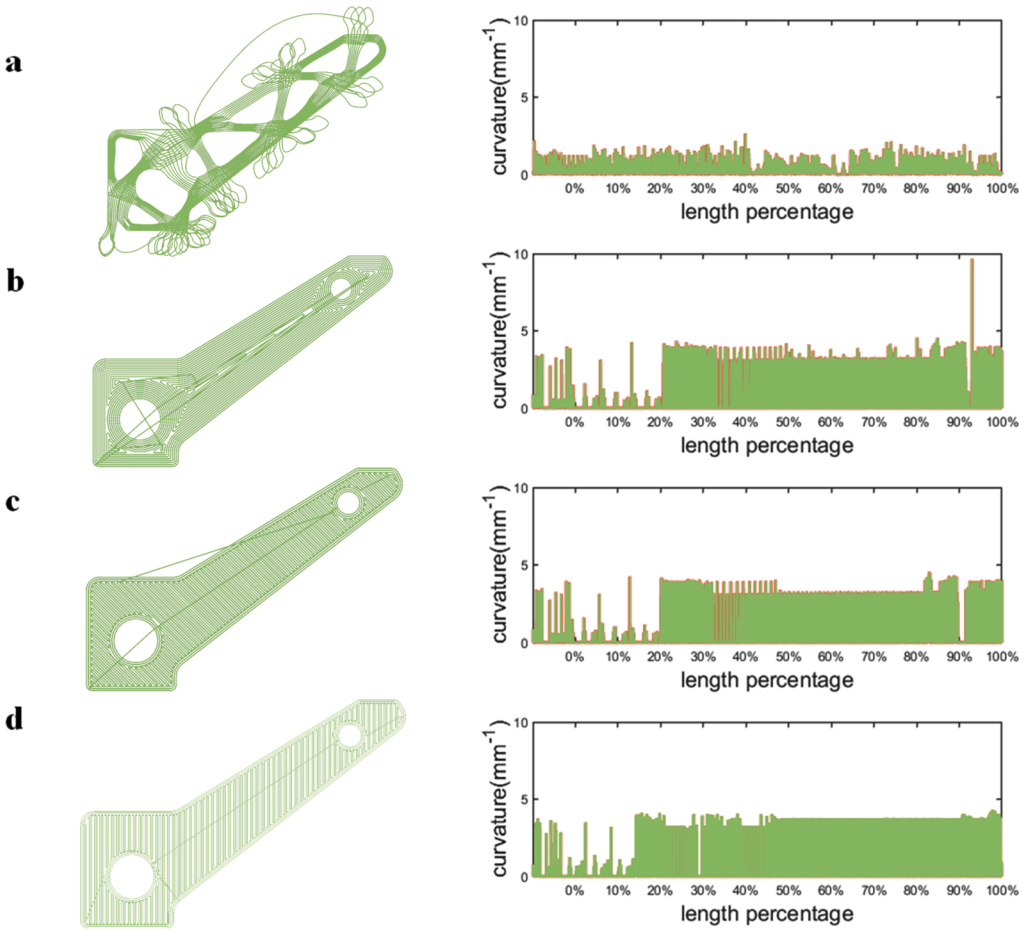

Fig. 9. Curvature distribution of different printing paths of the suspension part: (a) to (d) curvature distribution of the LPP, concentric, 45° zigzag and 90° zigzag printing paths.

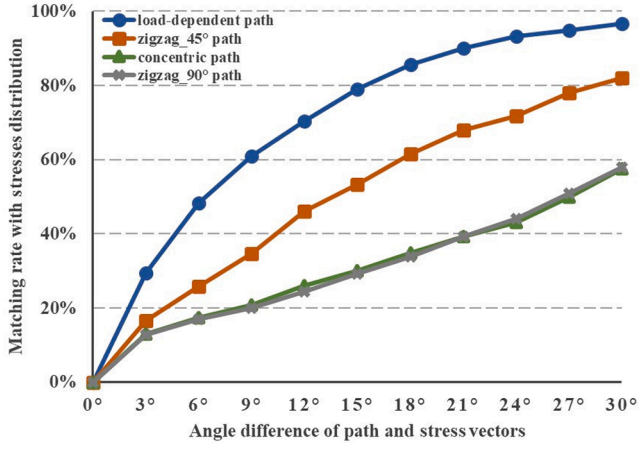

Fig. 10. Matching rate of different printing paths of the three-points-bending bridge part according to various angle difference of path and stress vectors.

stresses and printing path is represented by the angle between them. By counting how many path vectors are in the range of angle difference with adjacent stress vectors, the matching rate between the printing path and the stress distribution can be generally estimated. As shown in Fig. 10, the LPP printing path of the bridge part has the highest matching rate than the other printing paths generated by Slic3r. As a result of the diverse filling patterns of the printing paths generated by Slic3r, the matching rate of each printing path is different. With reference to the stress distribution of the original bridge part (shown in Fig. 5(a)), the direction of the principal stress vectors around the hole is distributed along the boundary. Thus, the 45° zigzag printing path accidentally has some paths that fit the load transmission paths. On the contrary, the 90° zigzag and concentric printing paths can hardly match the stress vectors.

With the increase of angle difference range, the matching rate of the LPP path is increased progressively. The variable spacing between adjacent paths allows the generated paths to follow the principal stresses adaptively. The other printing paths generated by Slic3r are partially matched with the stress distribution because some sporadic principal stresses vectors have a small angle difference with the nearby printing path by coincidence. It is worth to be mentioned that for the path of the three-points-bending bridge part about 96.6% of the printing path vectors of the LPP path have less than 30° angle difference with the principal stress vectors. As shown in Fig. 11, the LPP path of the suspension part has about 20% higher matching rate with the stress vectors than other printing paths of Slic3r. Meanwhile, the 90° zigzag printing path has nearly no congruity with the principal stress distribution and shows the lowest matching rate.

3.3. Comparison of LPP with state-of-the-art path planning method of CFRPs

Currently, several path planning methods for topology optimized structures are developed and discussed by researchers. The printing paths of a topology optimized cantilever beam generated by using streamline method, offset method and Equally-Space method (EQS) are shown in Fig. 12(b), (c) and (d). For this cantilever beam, the left side is fixed and a load that points to the ground is applied on the right side of

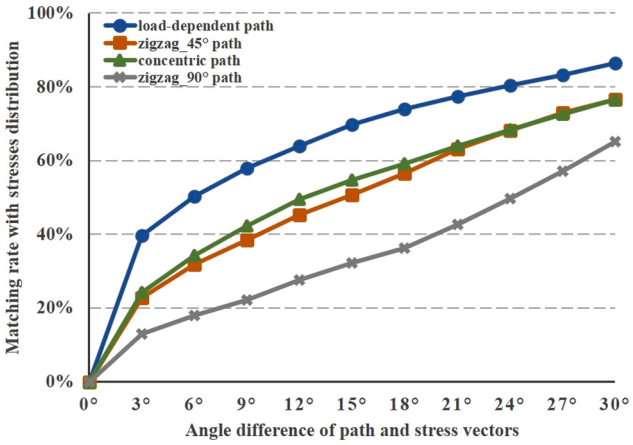

Fig. 11. Matching rate of different printing paths of the suspension part according to various angle difference of path and stress vectors.

the beam, as shown in Fig. 12(a). Obviously, the offset method generated interrupted paths, which cannot be used for continuous fiber printing. Meanwhile, the path contains too many sharp turns, which may lead to a high possibility of fiber fracture. The generated printing paths of streamline and EQS methods (Fig. 12(b) and (d)) have smooth turns and continuous load transfer benefits, but the joint areas have no connections. The joint area, such as the middle of the cantilever beam, exactly indicates a complex stress distribution and requires printing paths from different directions.

As shown in Fig. 13(a), under the load conditions mentioned above, two different kinds of stresses can be found inside the part. The blue one is the tensile stress and the green one is the compressive stress. The load paths based on the medial axis of the structure has been extracted by using the stress vector tracing algorithm and marked in the figure. The load-dependent printing path generated by LPP has shown in Fig. 13(b), and it is obvious that the geometrical edges have been followed with same shape and the printing path can pave the continuous fiber along the two stress vectors without compromise. The important joint areas are covered by the paths that go cross each other to achieve a better bonding and reinforcing properties. That means the joint areas have higher degree of compaction than other areas, due to the same layer thickness requirement of printing process.

Without loss of generality, an M-shape part and an L-shape part are also evaluated and discussed. For the M-shape part, the left and right sides of the bottom are fixed and a force is applied in the middle, as illustrated in Fig. 14(a). Meanwhile, the top side of the L-shape part is fixed and a force is applied on the middle point of the right side, as shown in Fig. 16(a). The printing paths of these two parts generated by EQS, streamline and Offset methods are shown in Figs. 14 and 16, respectively.

The printing paths of the M-shape part generated by the EQS method and streamline method can hardly fill the shape, especially at the corners, and the discontinuous offset printing path has too many sharp turns. As shown in Fig. 15(b), the LPP generated printing path has fully occupied the shape and are distributed along the principal stress transfer direction. The blue and green arrows in Fig. 15(a) represent the main distribution directions of the tensile and compressive stresses.

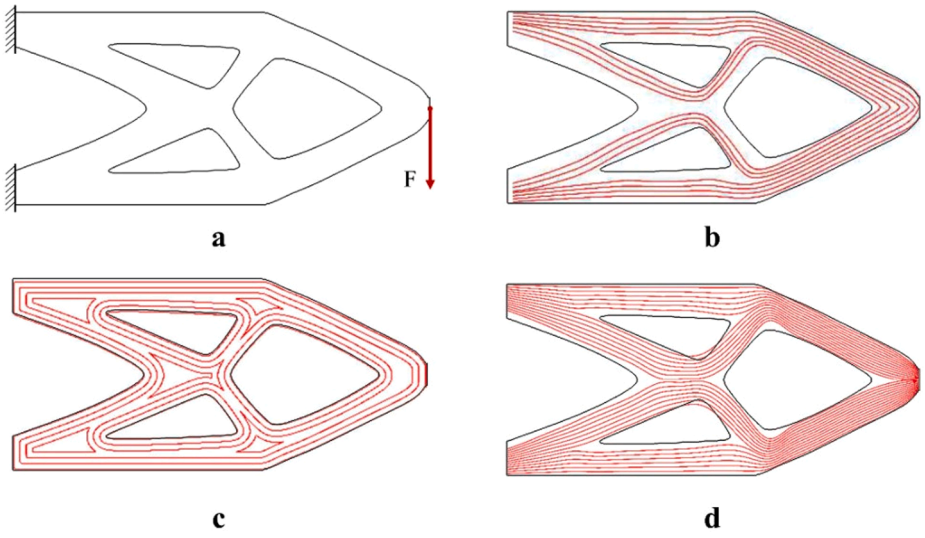

Fig. 12. Printing paths of topology optimized cantilever beam [36]: (a) load and supports condition; (b) path generated by streamline method; (c) path generated by offset method; (d) path generated by EQS method.

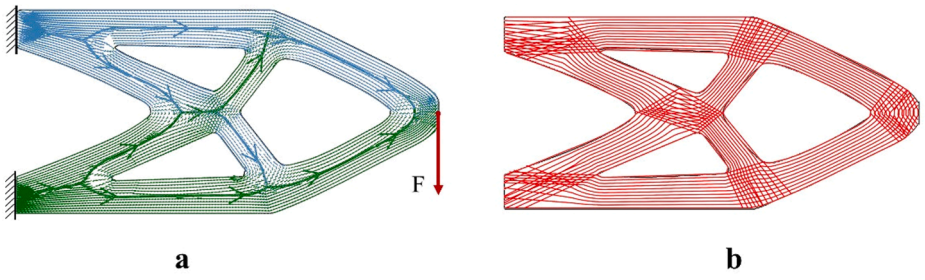

Fig. 13. LPP generated printing paths of topology optimized cantilever beam: (a) main transfer directions of the stress distribution; (b) LPP generated printing path based on stress distribution.

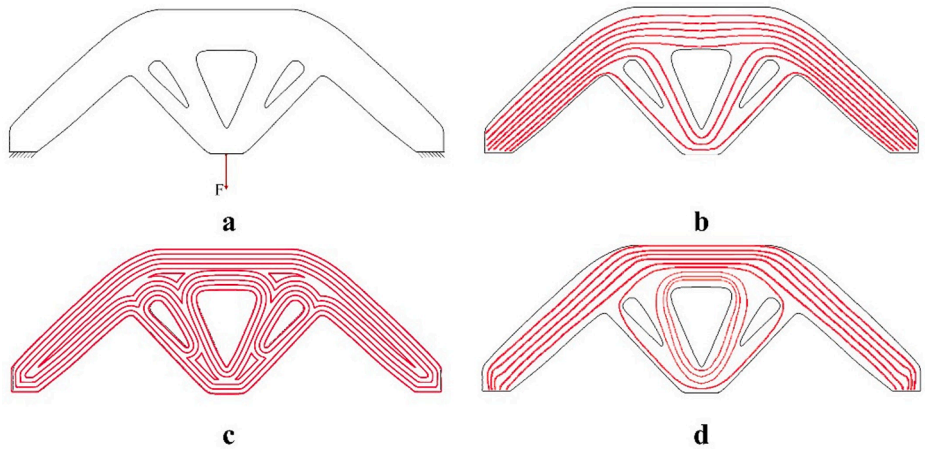

Fig. 14. Printing paths of topology optimized M-shape part [36]: (a) applied point load and supports condition; (b) path generated by EQS method; (c) path generated by offset method; (d) path generated by streamline method.

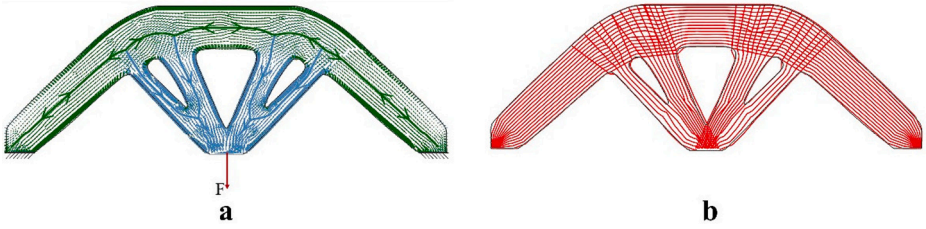

Fig. 15. LPP generated printing paths of topology optimized M-shape part: (a) main transfer directions of the stress distribution; (b) LPP generated printing path based on stresses distribution.

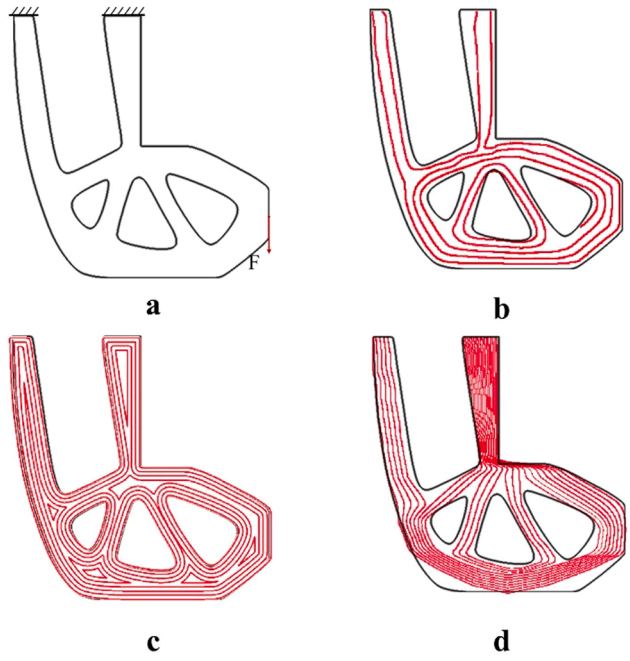

Fig. 16. Printing paths of topology optimized L-shape part [36]: (a) applied point load and supports condition; (b) path generated by streamline method; (c) path generated by offset method; (d) path generated by EQS method.

The printing paths of topology optimized L-shape part by using streamline, offset and EQS methods are shown in Fig. 16(b), (c) and (d). As discussed above, the offset printing path can fill the whole structure, but contains interrupted paths and sharp corners. For the EQS printing path, there are lots of blank areas between the paths and the geometrical edges, and the paths are non-uniformly distributed which causes excessive material depositing in the high-density path areas. The streamline printing path has the problem of shape distortion which occurs mainly around holes and disrupts the continuity of stress transmission paths. The LPP printing path of topology optimized L-shape part is shown in Fig. 17(a). Evidently, the LPP path follows the vectors of tensile and compressive stresses and fills the whole part with variable spacing of the adjacent paths. As a continuous printing path, there is only one starting point and one finishing point as marked in the figure. The red paths inside the printing area have been connected by the blue one, which is same as the three-point bending bridge and suspension parts. As shown in Fig. 17(b), a L-shape part reinforced by continuous carbon fibers has been manufactured by using 3D microwave printing technology and it has the same geometry as the LPP path.

4. Conclusion

In this work, a load-dependent 3D printing path planning method of continuous fiber reinforced plastics has been proposed. By using the topological optimization method, the load transmission paths are reordered and extracted. Then the developed Stress Vector Tracing algorithm has been used to generate the continuous load-dependent printing path of CFRPs from the extracted features, which contain geometry and stress vectors. Based on this method, the continuous fibers are printed along the load transmission path with high printing speed, variable spacing and low curvature turns. Several testing examples have been studied to verify the developed method. The result shows that the load-dependent 3D printing path planning method has the highest matching rate with the stress distribution. The state-of-the-art path planning method for continuous fiber reinforced plastics have been compared with our method. No matter the offset or EQS methods show a defective geometry filling pattern and discontinuous printing path which cannot

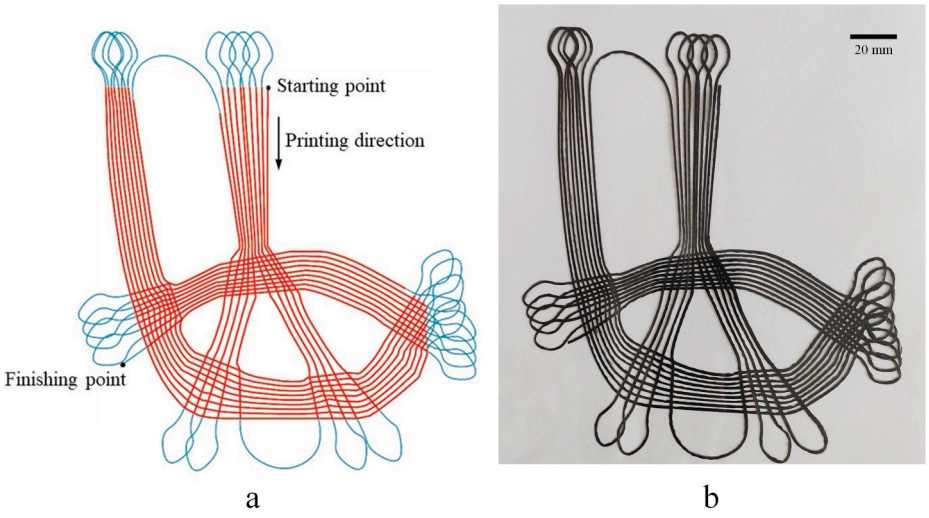

Fig. 17. (a) LPP generated printing paths of topology optimized L-shape part; (b) printed L-shape part with continuous carbon fiber reinforced polyamide filaments.

follow the load transmission. Lots of high curvature corners also prevent the availability of these paths. In future, the mechanical tests of the printed parts will be implemented to verify their mechanical properties.

CRediT authorship contribution statement

Ting Wang: Writing - original draft, Formal analysis, Methodology, Software. **Nanya Li:** Conceptualization, Writing - original draft, Methodology, Supervision. **Guido Link:** Investigation, Writing - review & editing. **John Jelonnek:** Resources, Supervision. **Jürgen Fleischer:** Resources, Supervision. **Jörg Dittus:** Writing - review & editing. **Daniel Kupzik:** Writing - review & editing.

Declaration of Competing Interest

The authors declare that they have no known competing financial interests or personal relationships that could have appeared to influence the work reported in this paper.

Acknowledgements

The authors would like to thank the support of Alexander von Humboldt Foundation as well as to the donor, the German Federal Ministry for Education and Research.

References

[1] Wang X, Jiang M, Zhou Z, Gou J, Hui D. 3D printing of polymer matrix composites: a review and prospective. Compos B Eng 2017;110:442–58.
[2] Brenken B, Barocio E, Favaloro A, Kunc V, Pipes RB. Fused filament fabrication of fiber-reinforced polymers: a review. Addit Manuf 2018;21:1–16.
[3] Agarwal K, Kuchipudi SK, Girard B, Houser M. Mechanical properties of fiber reinforced polymer composites: a comparative study of conventional and additive manufacturing methods. J Compos Mater 2018;52(23):3173–81.
[4] Ning F, Cong W, Qiu J, Wei J, Wang S. Additive manufacturing of carbon fiber reinforced thermoplastic composites using fused deposition modeling. Compos B Eng 2015;80:369–78.
[5] Baumann F, Scholz J, Fleischer J. Investigation of a new approach for additively manufactured continuous fiber-reinforced polymers. Procedia CIRP 2017;66:323–8.
[6] Li N, Li Y, Liu S. Rapid prototyping of continuous carbon fiber reinforced polylactic acid composites by 3D printing. J Mater Process Technol 2016;238:218–25.
[7] Li N, Link G, Jelonnek J. Rapid 3D microwave printing of continuous carbon fiber reinforced plastics. CIRP Ann 2020.
[8] Zhang H, Liu D, Huang T, Hu Q, Lammer H. Three-dimensional printing of continuous flax fiber-reinforced thermoplastic composites by five-axis machine. Materials 2020;13(7):1–11.
[9] Tekinalp HL, Kunc V, Velez-Garcia GM, Duty CE, Love LJ, Naskar AK, et al. Highly oriented carbon fiber-polymer composites via additive manufacturing. Compos Sci Technol 2014;105:144–50.
[10] Akhoundi B, Behravesh A. Effect of filling pattern on the tensile and flexural mechanical properties of FDM 3D printed products. Exp Mech 2019;59(6):883–97.
[11] Fidan I, Imeri A, Gupta A, Hasanov S, Nasirov A, Elliott A, et al. The trends and challenges of fiber reinforced additive manufacturing. Int J Adv Manufact Technol 2019;102(5–8):1801–18.
[12] Heidari-Rarani M, Rafiee-Afarani M, Zahedi A. Mechanical characterization of FDM 3D printing of continuous carbon fiber reinforced PLA composites. Compos B Eng 2019;175:1–8.
[13] Dutra TA, Ferreira RTL, Resende HB, Guimarães A. Mechanical characterization and asymptotic homogenization of 3D-printed continuous carbon fiber-reinforced thermoplastic. J Braz Soc Mech Sci Eng 2019;41(3):1–15.
[14] Akhoundi B, Behravesh AH, Bagheri SA. An innovative design approach in three-dimensional printing of continuous fiber–reinforced thermoplastic composites via fused deposition modeling process: In-melt simultaneous impregnation. Proc Inst Mech B: J Eng Manufact 2020;234(1–2):243–59.
[15] Mohammadizadeh M, Imeri A, Fidan I, Elkelany M. 3D printed fiber reinforced polymer composites-structural analysis. Compos B Eng 2019;175:1–6.
[16] Naranjo-Lozada J, Ahuett-Garza H, Orta-Castañón P, Verbeeten WM, Sáiz-González D. Tensile properties and failure behavior of chopped and continuous carbon fiber composites produced by additive manufacturing. Addit Manuf 2019;26:227–41.
[17] Kousiatza C, Tzetzis D, Karalekas D. In-situ characterization of 3D printed continuous fiber reinforced composites: a methodological study using fiber Bragg grating sensors. Compos Sci Technol 2019;174:134–41.
[18] Ye W, Lin G, Wu W, Geng P, Hu X, Gao Z, et al. Separated 3D printing of continuous carbon fiber reinforced thermoplastic polyimide. Compos A Appl Sci Manuf 2019;121:457–64.
[19] Todoroki A, Oasada T, Mizutani Y, Suzuki Y, Ueda M, Matsuzaki R, et al. Tensile property evaluations of 3D printed continuous carbon fiber reinforced thermoplastic composites. Adv Compos Mater 2020;29(2):147–62.
[20] Ivey M, Melenka GW, Carey JP, Ayranci C. Characterizing short-fiber-reinforced composites produced using additive manufacturing. Adv Manuf Polym Compos Sci 2017;3(3):81–91.
[21] Ming Y, Duan Y, Wang B, Xiao H, Zhang X. A novel route to fabricate high-performance 3D printed continuous fiber-reinforced thermosetting polymer composites. Materials 2019;12(9):1–13.
[22] Liu T, Tian X, Zhang Y, Cao Y, Li D. High-pressure interfacial impregnation by micro-screw in-situ extrusion for 3D printed continuous carbon fiber reinforced nylon composites. Compos A Appl Sci Manuf 2020;130:1–9.
[23] Quan C, Han B, Hou Z, Zhang Q, Tian X, Lu TJ. 3d printed continuous fiber reinforced composite auxetic honeycomb structures. Compos B Eng 2020;187:1–12.
[24] Dickson AN, Barry JN, McDonnell KA, Dowling DP. Fabrication of continuous carbon, glass and Kevlar fibre reinforced polymer composites using additive manufacturing. Addit Manuf 2017;16:146–52.
[25] Adumitroaie A, Antonov F, Khaziev A, Azarov A, Golubev M, Vasiliev VV. Novel continuous fiber Bi-matrix composite 3-D printing technology. Materials 2019;12(18):1–10.
[26] De Backer W, Sinkez P, Chhabra I, Van Tooren MJ, Bergs A. In-process monitoring of continuous fiber additive manufacturing through force/torque sensing on the nozzle. AIAA Scitech 2020 Forum 2020.
[27] Eichenhofer M, Wong JC, Ermanni P. Continuous lattice fabrication of ultra-lightweight composite structures. Addit Manuf 2017;18:48–57.
[28] Liu S, Li Y, Li N. A novel free-hanging 3D printing method for continuous carbon fiber reinforced thermoplastic lattice truss core structures. Mater Des 2018;137:235–44.

[29] Shembekar AV, Yoon YJ, Kanyuck A, Gupta SK. Generating robot trajectories for conformal three-dimensional printing using nonplanar layers. J Comput Inf Sci Eng 2019;19(3):1–13.
[30] Sugiyama K, Matsuzaki R, Malakhov AV, Polilov AN, Ueda M, Todoroki A, et al. 3D printing of optimized composites with variable fiber volume fraction and stiffness using continuous fiber. Compos Sci Technol 2020;186. https://doi.org/10.1016/j.compscitech.2019.107905.
[31] Li N, Link G, Wang T, Ramopoulos V, Neumaier D, Hofele J, et al. Path-designed 3D printing for topological optimized continuous carbon fibre reinforced composite structures. Compos B Eng 2020;182. https://doi.org/10.1016/j.compositesb.2019.107612.
[32] Fernandez-Vicente M, Calle W, Ferrandiz S, Conejero A. Effect of infill parameters on tensile mechanical behavior in desktop 3D printing. 3D printing and additive manufacturing. 2016;3(3):183–192.
[33] Sharma M, Rao IM, Bijwe J. Influence of fiber orientation on abrasive wear of unidirectionally reinforced carbon fiber–polyetherimide composites. Tribol Int 2010;43(5–6):959–64.
[34] Bendsoe MP, Sigmund O. Topology optimization: theory, methods, and applications. Springer Science & Business Media; 2013.
[35] Kenedi PP, Vignoli LL, Duarte BT, Matos FCA, Dias HOT. Orthotropic elastic properties assessment of sandwich laminates. J Aerospace Technol Manage 2017;9(3):389–96.
[36] Papapetrou VS, Patel C, Tamijani AY. Stiffness-based optimization framework for the topology and fiber paths of continuous fiber composites. Compos B Eng 2020;183. https://doi.org/10.1016/j.compositesb.2019.107681.
[37] Lee D-T. Medial axis transformation of a planar shape. IEEE Trans Pattern Anal Mach Intell 1982;4:363–9.